An XAS Investigation of Product and Inhibitor Complexes of Ni-Containing GlxI from *Escherichia coli*: Mechanistic Implications†

Gerard Davidson,§ Susan L. Clugston,‡ John F. Honek,‡ and Michael J. Maroney*,§

Department of Chemistry, University of Massachusetts, Amherst, Massachusetts 01003 and the Department of Chemistry, University of Waterloo, Waterloo, Ontario, N2L 3G1

Received August 8, 2000; Revised Manuscript Received February 9, 2001

ABSTRACT: *Escherichia coli* glyoxalase I (GlxI) is a metalloisomerase that is maximally activated by Ni^{2+}, unlike other known GlxI enzymes which are active with Zn^{2+}. The metal is coordinated by two aqua ligands, two histidines (5 and 74), and two glutamates (56 and 122). The mechanism of *E. coli* Ni-GlxI was investigated by analyzing Ni K-edge X-ray absorption spectroscopic (XAS) data obtained from the enzyme and complexes formed with the product, *S*-D-lactoylglutathione, and various inhibitors. The analysis of X-ray absorption near edge structure (XANES) was used to determine the coordination number and geometry of the Ni site in the various Ni-GlxI complexes. Metric details of the Ni site structure were obtained from the analysis of extended X-ray absorption fine structure (EXAFS). Interaction of *S*-D-lactoylglutathione (product) or octylglutathione with the enzyme did not change the structure of the Ni site. However, analysis of XAS data obtained from a complex formed with a peptide hydroxamate bound to Ni-GlxI is consistent with this inhibitor binding to the Ni center by displacement of both water molecules. XANES analysis of this complex is best fit with a five-coordinate metal and, given the fact that both histidine ligands are retained, suggests the loss of a glutamate ligand. The loss of a glutamate ligand would preserve the neutral charge on the Ni complex and is consistent with the lack of a significant shift in the Ni K-edge energy in this complex. These data are compared with data obtained from the *E. coli* Ni-GlxI selenomethionine-substituted enzyme. The replacement of three methionine residues in the native enzyme with selenomethionine does not affect the structure of the Ni site. However, addition of the peptide hydroxamate inhibitor leads to the formation of a complex whose structure as determined by XAS analysis is consistent with inhibitor binding via displacement of both water molecules but retention of both histidine and glutamate ligands. This leads to an anionic complex, which is consistent with an observed 1.7 eV decrease in the Ni K-edge energy. Plausible reaction mechanisms for Ni-GlxI are discussed in light of the structural information available.

Methylglyoxal (MG)[1] is a normal cellular metabolite, yet is cytotoxic at millimolar concentrations (*1*). It is formed either enzymatically, by methylglyoxal synthase, triosephosphate isomerase, or via the catabolism of threonine, or nonenzymatically from dihydroxyacetone phosphate (*1*). The major precursors of MG are glyceraldehyde-3-phosphate and dihydroxyacetone phosphate, which are both derived from glycolysis (*2*). Several possible mechanisms for the cytotoxicity of MG have been reported, including the formation of MG-DNA/RNA adducts, inhibition of protein synthesis, and modification of proteins (*1*, *3*−*5*). In addition, MG has been shown to act as both a mutagen and a carcinogen (*6*). Nature, however, has devised a method for the detoxification of cytotoxic MG and other toxic 2-oxoaldehydes: the glyoxalase system (*1*). The glyoxalase system functions by converting the hemimercaptal formed from the nonenzymatic reaction of glutathione (GSH) and MG into D-lactate. The first step in the process is the conversion of the hemimercaptal to the thioester of D-lactate (Scheme 1) and is catalyzed by glyoxalase I (GlxI, *S*-D-lactoylglutathione lyase, EC 4.4.1.5) (*5*, *7*).

Of the GlxI enzymes studied to date, all have been shown to require a metal for activity (*7*). The enzymes obtained from *Homo sapiens*, *Saccharomyces cerevisiae*, and *Pseudomonas putida* are all active in the presence of Zn^{2+} (*8*−*10*). The enzyme from *Escherichia coli*, however, has maximal activity in the presence of Ni^{2+}, but is inactive with Zn^{2+}, and therefore constitutes the first example of a Ni-bound

† This research was supported by grants from the National Institutes of Health (GM38829, M.J.M.) and NSERC of Canada (J.F.H.). S.L.C. was supported by a postgraduate scholarship from NSERC. Data were collected at the National Synchrotron Light Source (NSLS) Brookhaven National Laboratory, which is supported by the U.S. Department of Energy, Division of Materials Sciences and Division of Chemical Sciences. Beamline X9B at NSLS is supported in part by NIH Grant RR-01633.

* To whom correspondence should be addressed. Professor Michael J. Maroney, Department of Chemistry, Lederle Graduate Research Center Tower A, University of Massachusetts, Amherst, MA 01003-4510. Phone: 413-545-4876. Fax: 413-545-4490. E-mail: Mmaroney@chem.umass.edu.

§ University of Massachusetts.

‡ University of Waterloo.

[1] Abbreviations: EPR, electron paramagnetic resonance; EXAFS, extended X-ray absorption fine structure; GlxI, glyoxalase I; GSH, glutathione; HOX, L-γ-glutamyl-*N*-hydroxy-*N*-methyl-L-glutaminylglycine; LacGSH, *S*-D-lactoylglutathione; MG, methylglyoxal; OctylGSH, *S*-octylglutathione; SeMet, selenomethionine; tmen, *N*,*N*,*N*′,*N*′-tetramethylethylenediamine; XANES, X-ray absorption near edge structure; XAS, X-ray absorption spectroscopy.

10.1021/bi0018537 CCC: $20.00
Published on Web 03/22/2001

Scheme 1

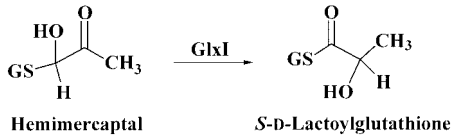

isomerase (Ni-GlxI) (*11*). Sequence homology between the *E. coli* enzyme and putative GlxI genes in a number of pathogenic bacteria suggest that GlxI may be a new target for the development of antimicrobial agents (*12*).

The reported X-ray crystal structure of human GlxI reveals an octahedral Zn site that is coordinated by residues Gln33, Glu99, His126, Glu172, and a water molecule at 2.1 Å (*13*). A second water molecule located 2.8 Å from the Zn completes a distorted six-coordinate environment (*14*, *15*). Although *E. coli* GlxI has only 36% sequence identity with *H. sapiens* GlxI, three of the four metal ligands are conserved (Glu56, Glu122, and His74) (*11*). The fourth ligand in *E. coli* Ni-GlxI was tentatively assigned to His5, replacing Gln33 in *H. sapiens* based on sequence homology. A preliminary X-ray absorption spectroscopy (XAS) study of *E. coli* Ni-GlxI has been communicated, and the results are consistent with the presence of two His residues in the Ni coordination environment and a likely active site structure, $[Ni(His)_2(Glu)_2(OH_2)_2]$ (*16*). This structure was recently confirmed and detailed further with the publication of the 1.5-Å resolution crystal structure of *E. coli* Ni-GlxI (*17*). The crystal structure reveals an octahedral Ni site coordinated by residues His5, Glu56, His74, Glu122, and two water molecules located at 2.1 and 2.2 Å, respectively. It was observed that substitution of Zn for Ni in *E. coli* GlxI leads to a loss of activity, and the cause of inactivation was investigated using XAS and X-ray crystallography. The initial XAS results suggested that a water molecule was lost upon substitution with Zn to obtain a $[Zn(His)_2(Glu)_2(OH_2)]$ site and confirmed by the 1.8-Å resolution crystal structure (*17*). The crystal structure reveals a trigonal bipyramidal Zn site coordinated by residues His5, Glu56, His74, Glu122, and a water molecule at 2.0 Å.

The GlxI reaction mechanism has been the focus of some debate. It has been suggested on the basis of solvent isotope exchange studies, that proton abstraction from the substrate allows the formation of an enediol(ate) that can then be reprotonated at the adjacent carbon (*18*). The catalytic role of the metal in this process is not yet clear. Direct metal interaction with the enediol(ate) oxygen atoms has been proposed (*14*), as has the activation of metal-bound water molecules (*19*, *20*). An observation from structural studies of GlxI is the apparent importance of the number of water molecules bound at the active site. *E. coli* Ni-GlxI and *H. sapiens* GlxI both possess two water molecules at the metal site (*14*, *16*). Since substitution of Zn^{2+} for Ni^{2+} in *E. coli* GlxI leads to a change in the coordination environment of the metal and a water molecule is lost, in addition to the loss of enzyme activity, it is possible that two water molecules are required at the active site for isomerase activity. This hypothesis is supported by previous studies on *H. sapiens* GlxI that highlighted the importance of having two water molecules interacting with the substrate (*19*, *20*).

Attempts to resolve the mechanism have incorporated the use of putative transition state analogue (TSA) inhibitors and

Scheme 2

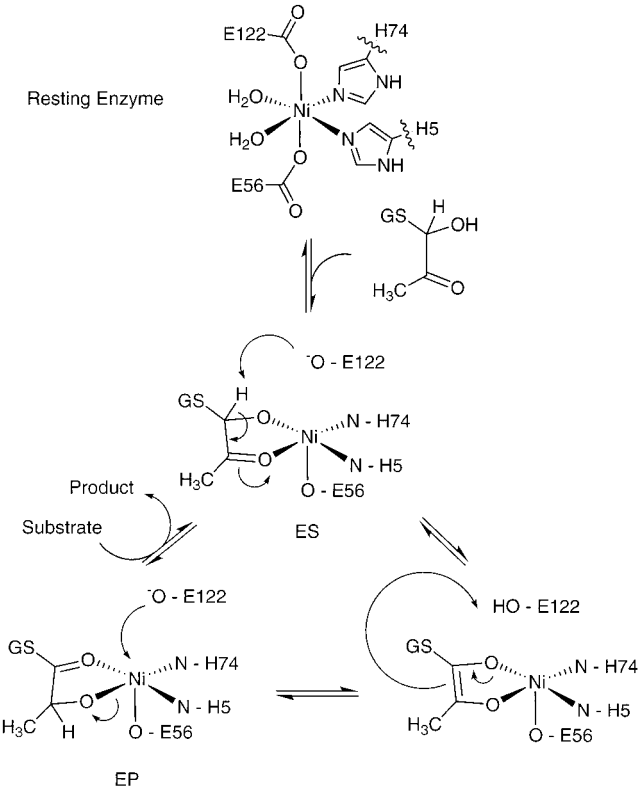

their structural effects on the metal site. The crystal structure of *H. sapiens* GlxI in the presence of the transition state analogue inhibitor, *S*-(*N*-hydroxy-*N*-*p*-iodophenylcarbamoyl)-glutathione, indicates that two water molecules and Glu172 are displaced by the two O atoms from the inhibitor to produce a five-coordinate Zn site (*14*). The mechanism proposed to account for this observation requires conversion of a six-coordinate Zn site to a five-coordinate site upon addition of substrate. Substrate binding involves replacement of the two water molecules by the two O atoms from the enediol(ate) substrate and displacement of Glu172. This allows the displaced Glu172 to act as a catalytic base.

Three possible mechanisms can be considered for *E. coli* GlxI (Schemes 2−4): Addition of substrate results in displacement of a water molecule(s) and Glu122 (Glu172 in *H. sapiens*), which could then act as a catalytic base once displaced, in analogy with that proposed for *H. sapiens* (Scheme 2). One or both water molecules on the metal are deprotonated and act as proton abstractors (Scheme 3). An unknown side chain acts as the catalytic base, either with the water molecules on the metal polarizing the substrate (shown) or directly displacing the two oxygen atoms in the substrate (Scheme 4). The purpose of this XAS study was to examine the behavior of the Ni site in *E. coli* Ni-GlxI after the addition of either the reaction product or one of two different inhibitors (Scheme 5). Of particular interest is the effect on the number of histidine (His) and carboxylate residues coordinated in these complexes. This aspect is addressed by using EXAFS analysis with multiple scattering to examine features arising from second coordination sphere C atoms. In addition to the wild-type enzyme, the seleno-methionine derivative of *E. coli* GlxI, where three Met residues (Met 1, 7, and 26) were replaced with SeMet, was studied. This derivative has a slightly modified V_{max}. Since

Scheme 3

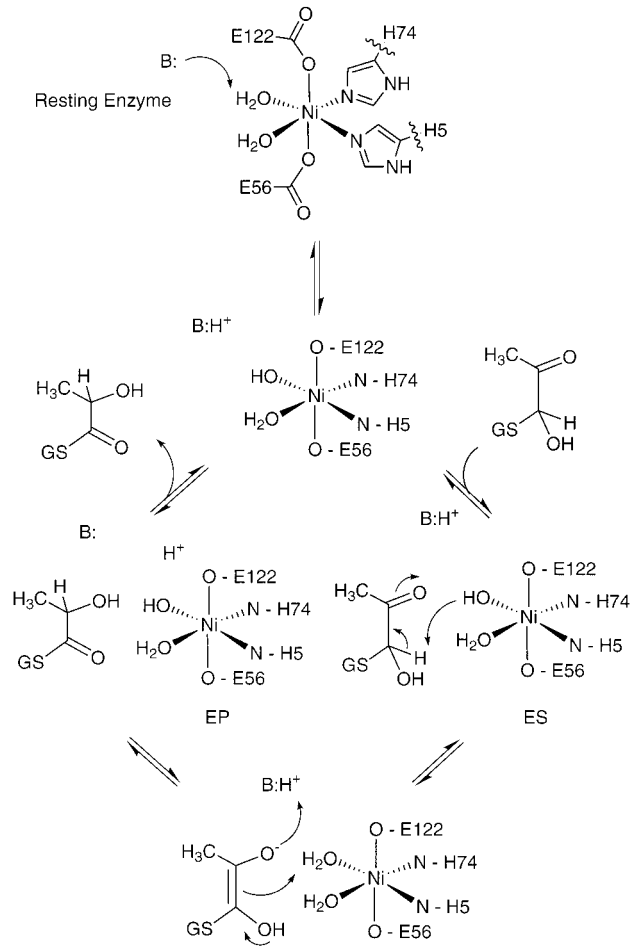

SeMet substitution does not often alter enzyme kinetics, it was interesting to also study this protein to elucidate the structural role played by SeMet. This is important in *E. coli* GlxI, since in the recently elucidated crystal structure of the enzyme Met 7 is in spatial proximity to the Ni active site. Thus, we have included the SeMet-substituted enzyme in this study to determine the nature of the structural perturbation of the Ni site that occurs upon substitution of S by Se.

EXPERIMENTAL PROCEDURES

Protein Production, Purification, and Selenomethionine Incorporation. Native GlxI expression and purification was performed as previously described (*11*). Initially, a methionine auxotrophic cell line *E. coli* DH93 (MG1655 *metH*174::*Tn*5 *metE*::*Tn*10; laboratory collection) was used for the expression of GlxI in the presence of seleno-L-methionine (SeMet; Sigma Chemical Co.). This proved ineffective for GlxI protein production, even in the presence of normal methionine. The system used for the expression of wild-type GlxI [*E. coli* MG1655/pGL10 (*11*)] was also successfully used for the incorporation of SeMet when grown in minimal media (M9, ref *21*), supplemented with 0.4% glucose, 1 mM $MgSO_4$, 0.1 mM $CaCl_2$, 0.001% uracil, and 5 μM $NiCl_2$.

For SeMet incorporation, a LB_{Amp} starter culture was inoculated with *E. coli* MG1655/pGL10 and allowed to grow for ~8 h at 37 °C. This was used to directly inoculate (1:100 dilution) 0.7 L warm M9. After reaching an OD_{600} of ~0.5, SeMet (final concentration 0.3 mM) and additional $NiCl_2$ (to a final concentration of 12.5 μM) were added. The culture was allowed to grow for another 30 min prior to induction of protein synthesis (8 h with 0.5 mM IPTG). The cells were harvested, and the SeMet protein was purified in the same manner as the native enzyme (*11*).

Electrospray mass spectrometry (ESMS; Figure 1) provided by the Biological Mass Spectrometry Laboratory, University of Waterloo, was utilized to monitor the level of SeMet incorporation.

EPR spectra were obtained on a Bruker ESR300-E spectrometer at 77 K in a finger dewar.

The kinetic analysis of the SeMet GlxI derivative was performed utilizing the previously described enzymatic assay (*11*) measuring the activity at 10 substrate concentrations between 0.01 and 2.0 mM with purified *E. coli* SeMet GlxI activated with 2.5 mol equivalence of nickel to dimeric enzyme.

Enzyme and XAS Sample Preparation. Sample preparation and data collection for Ni-GlxI has been previously reported (*16*). The Ni-GlxI samples used to prepare the product and inhibitor complexes were prepared as follows. Ni-GlxI was prepared as previously described by adding 1.5× molar equivalents of $NiCl_2$ to purified recombinant apoenzyme (*11*). The protein was then concentrated using a Centricon concentrator (Amicon; YM10). The buffer was changed three times to 50 mM MOPS, 25% glycerol, and the pH was adjusted to 7.0 using tetraethylammonium hydroxide (10% solution in water). The enzyme preparation was then split into three aliquots for addition of the different product/inhibitor complexes. The enzyme−product complex was prepared by adding *S*-D-lactoylglutathione (LacGSH; to a final concentration of 5 mM) in 50 mM MOPS and 25% glycerol to one aliquot. The *S*-octylglutathione inhibitor complex was prepared by adding *S*-octylglutathione (OctylGSH; also to 5 mM final concentration) in 50 mM MOPS and 25% glycerol to a second aliquot. A second inhibitor complex was prepared by adding L-γ-glutamyl-*N*-hydroxy-*N*-methyl-L-glutaminylglycine (hydroxamate; to 10 mM final concentration) in water to the third aliquot. Sample three was diluted by the addition of a solution of hydroxamate in water, to give final concentrations of 40 mM MOPS and 20% glycerol. LacGSH and OctylGSH were obtained from Sigma Chemical Co., and the synthesis of the hydroxamate has been previously reported (*22*). The concentrations of LacGSH, OctylGSH, and hydroxamate used in EXAFS samples were higher than the determined IC_{50} values of these compounds (2.05 mM, 0.52 mM, and 1.80 μM, respectively, ref *23*).

XAS Data Collection and Analysis. XAS data for all samples were collected on beam line X9B at the National Synchroton Light Source (NSLS) at Brookhaven National Laboratory over several runs. The samples were contained in polycarbonate holders that were inserted into slotted aluminum holders held near 50 K using a He displex cryostat for XAS data collection. Data were collected under dedicated conditions at 2.58 GeV and 120−200 mA as previously described (*24*), using a Si(220) double crystal monochromator and internally calibrated to the first inflection point of Ni foil (8331.6 eV). This arrangement provides a theoretical resolution of ca. 0.5 eV for the 0.5-mm hutch slit height employed. The data from the SeMet Ni-GlxI hydroxamate complex were recorded in a similar manner except that a Si(111) double crystal monochromator was

Scheme 4

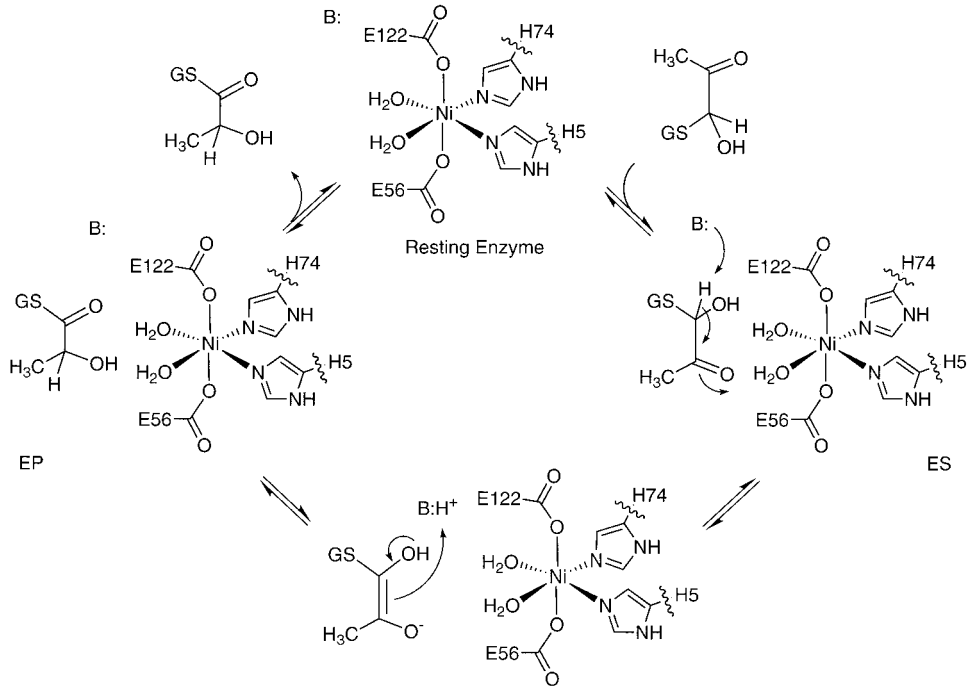

Scheme 5

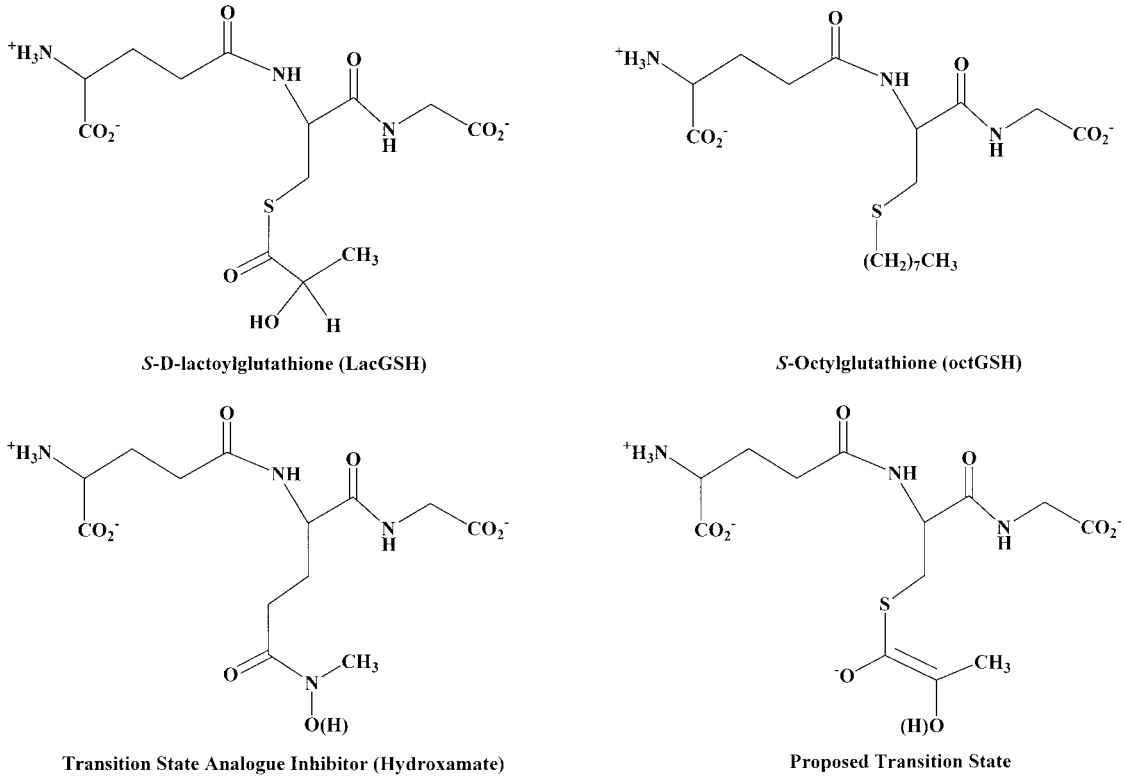

used. This provides a theoretical resolution of ca. 1.0 eV. Harmonic rejection was accomplished with a focusing mirror left flat. X-ray fluorescence data were collected using a 13-element Ge detector (Canberra). The integrity of the samples after ~10 h of exposure to monochromatic synchrotron radiation was determined by monitoring the Ni K-edge energy on sequential scans. No changes in either redox state or ligand environment were observed. Data for nickel(II) hexakisimidazole tetrafluoroborate $[Ni(Im)_6](BF_4)_2$ were collected and analyzed as previously described (*25*).

The XAS spectra reported are the sum of 14−16 scans and were analyzed in analogy with previously published procedures (*24*). For the purpose of comparison, the Ni K-edge energy of the samples was taken to be the energy at a normalized absorbance of 0.5 (Table 1). The edge values are reproducible to ± 0.1 eV. The areas under the peaks assigned to 1s → 3d transitions were determined by fitting a background to the region of the normalized spectrum immediately below and above this feature in energy and integrating the difference.

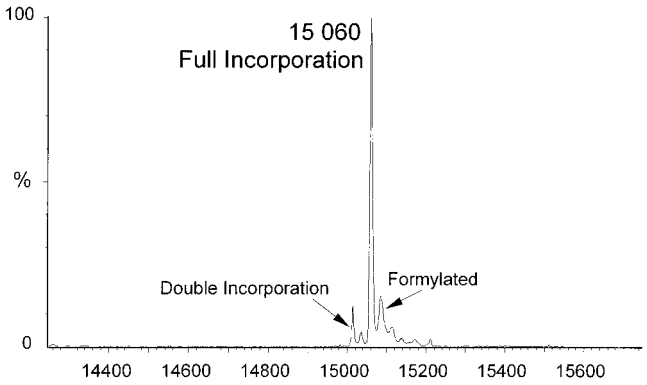

FIGURE 1: Reconstructed electrospray mass spectrum of the purified SeMet GlxI, showing the fully incorporated (three SeMet) protein with minor levels of double incorporated protein and formylated fully incorporated protein.

Table 1: Ni K-Edge and XANES Spectra for *Escherichia coli* Glyoxalase I

sample	Ni K-edge energy (eV)	1s → 3d peak area (10^{-2} eV)	ref
Ni-GlxI	8341.9(1)	2.8(5)	*16*
Ni-GlxI LacGSH complex	8341.9(1)	3.5(3)	this work
Ni-GlxI OctylGSH complex	8341.9(1)	3.6(5)	this work
Ni-GlxI hydroxamate complex	8341.7(1)	5.1(4)	this work
SeMet Ni-GlxI	8342.0(1)	3.8(2)	this work
SeMet Ni-GlxI hydroxamate complex	8340.3(1)	1.5(2)	this work

Extended X-ray absorption fine structure (EXAFS) data were analyzed using the XAS analysis package WINXAS (*26*). Analysis of EXAFS features arising from atoms in the first coordination sphere was accomplished as previously described (*27*). The summed, energy-calibrated data files were background-corrected and normalized using a two polynomial fit, with a first-order polynomial for the pre-edge region and a third-order polynomial for the post-edge region. The data were converted to *k*-space using the relationship $[2m_e(E - E_0)/\bar{h}^2]^{1/2}$, where m_e is the electron mass, E is the photon energy, $\bar{h}$ is Planck's constant divided by 2π, and E_0 is the threshold energy of the absorption edge and defined here as 8340.0 eV. A least-squares fitting procedure was employed over a k range of 2−12.5 Å^{-1} using Fourier-filtered EXAFS with a backtransform window of 1.1−4.0 Å (uncorrected for phase shifts). The data were truncated at $k = 12.5$ Å^{-1} because of the presence of trace amounts of Cu in the samples. The fitting procedure minimized GOF $= 1/\sigma^2\sum_{i=1}^{N}[y_{exp}(i) - y_{theo}(i)]^2$ (where σ is an estimate for the experimental error and y_{exp} and y_{theo} are experimental and theoretical data points, respectively, and N is the number of data points) (*26*). Comparison of residual values (*26*) (eq 1) and the difference in the disorder parameters between model data and the fit, $|\Delta\sigma^2| = |(\sigma^2_{fit} - \sigma^2_{model})|$, using the XAS formula (eq 2) (*26*) were used to select the best fits of the data (where σ^2_{model} is the disorder parameter obtained from FEFF 6 calculations of the relevant crystallographically characterized model compound). Thus, $\Delta\sigma^2$ values provide a comparison of the disorder in the enzyme with a well-ordered model system. The dynamic disorder in bond distances was minimized by recording spectra on samples held at 50 K in a He displex cryostat. Static disorder arises from small differences in Ni-X bond distances within the same shell. As a result, four well-ordered Ni-O/N distances can give a similar EXAFS amplitude as six less well-ordered Ni-O/N distances. This correlation effectively limits the accuracy of the determination of the number of scattering atoms (N) in a refined shell to ca. ± 25% or ± 1 donor atom. The correlation between N and σ^2 was minimized by constraining the number of scattering atoms to integer values and varying σ^2 to obtain the best fit of the amplitude.

$$\text{residual [\%]} = \frac{\sum_{i=1}^{N}|y_{exp}(i) - y_{theo}(i)|}{\sum_{i=1}^{N}|y_{exp}(i)|}\cdot 100 \quad (1)$$

$$\chi(k) = \sum_j \frac{N_j S_0{}^2 F_j(k)}{kR_j{}^2} e^{(-2k^2\sigma_j{}^2)} e^{(-2R_j/\lambda)} \sin[2kR_j + \delta_j(k)] \quad (2)$$

Theoretical phases and amplitudes for single scattering EXAFS analyses were obtained from FEFF 6 (*28*−*30*) calculations of crystallographically characterized model compounds as previously described (*16*, *27*). Theoretical phases and amplitudes for multiple scattering EXAFS analyses were also obtained from FEFF 6 using the crystallographically characterized model compounds diaqua-bis(salicylaldehydato) nickel(II) (*31*) $[Ni(sal)_2(H_2O)_2]$, $[Ni(Im)_6](BF_4)_2$ (*32*) and bis(L-lactato)(*N*,*N*,*N*′,*N*′-tetramethylethylenediamine nickel(II) $[Ni(lac)_2(tmen)]$ (*33*). Photoelectron scattering pathways were calculated out to a distance of 6.1 Å. In the case of $[Ni(sal)_2(H_2O)_2]$, the second coordination sphere C atoms produced only two scattering pathways, one single scattering path and one multiple scattering path with a 36% relative intensity (Table S1, Supporting Information). To simplify the fitting procedure, the distances for the two pathways involving the second coordination sphere C atoms were correlated so that only one adjustable distance (Ni-C) was involved in the fits. A single σ^2 value was used for both pathways. Modeling second coordination sphere C atoms with parameters from $[Ni(sal)_2(H_2O)_2]$ failed to converge in the case of complexes with the hydroxamate ligand, hox, so $[Ni(lac)_2(tmen)]$ was used as a more accurate model of these C atoms. Six pathways involving the C_α atoms of the lactato ligand were obtained from FEFF 6 calculations, two single and four multiple scattering paths. However, two of the multiple scattering pathways had relative intensities of <10% and were neglected to minimize the number of adjustable parameters used in the fits. The remaining two multiple scattering pathways had relative intensities of ∼26%. As in the case of second coordination sphere carboxylate C atoms, the distances for the two pathways were correlated so that only one adjustable distance (Ni-C) was involved in the fits. A single σ^2 value was used for all four pathways.

Single and multiple scattering pathways for $[Ni(Im)_6](BF_4)_2$ were obtained using a slightly different procedure. Instead of using all six imidazole rings from the crystal structure, only one ring was chosen as a basis and theoretical phases, and amplitudes were calculated from this single ring. Those pathways with a relative intensity ≥17% (all paths)

were used in the fitting procedure. FEFF 6 pathways were calculated to a distance of 6.1 Å, although the maximum distance of pathways that contributed significantly to the EXAFS was 4.448 Å. (See Supporting Information, Table S1.) This resulted in the use of 15 pathways to describe the EXAFS from an imidazole ring, one for the first coordination sphere N atom, four for the second coordination sphere C atoms, and 10 for the third coordination sphere C/N atoms. In fitting imidazole rings, the distances between N, second coordination sphere C, and third coordination sphere C and N atoms were correlated so that the ring refined as a unit with one adjustable Ni-N distance. Four values of σ^2 were used to describe the imidazole ring, one for atoms in the first coordination sphere (N), one for both C atoms in the second coordination sphere, and two for the C/N atoms in the third coordination sphere. The use of two disorder parameters to discriminate between pathways with distances of <4.35 Å and pathways with distances of >4.35 Å allowed for some adjustment in the importance of multiple scattering pathways in the fits of unknowns relative to the calculated models. Thus, large disorder parameters for certain pathways indicate a decreased importance of that path in fitting experimental data relative to the $[Ni(Im)_6]^{2+}$ model. The number of histidine ligands was determined from fits employing one, two, and three imidazole rings, which were not independently refined. The pathways are described in detail in the Supporting Information, Table S1.

Fourier filtered EXAFS data using a backtransform window of 1.1−4.0 Å (uncorrected for phase shifts) were fit using the following strategy: (i) The atoms in the first coordination sphere were first modeled as a single shell of scattering atoms, and the best fit using 4, 5, or 6 O/N (O parameters were used) or S donor-atoms was obtained. (ii) The first coordination sphere was then separated into two shells and fit using an integer combination of O/N or S atoms totaling 4, 5, or 6. (iii) Next, one of the O/N scatterers was replaced by an imidazole ring and the Ni-N distance and ring disorder parameters refined along with the parameters describing other first coordination sphere atoms. (iv) The number of imidazole rings was adjusted to give the best fit. (v) Last, additional second shell C atoms were added to model features associated with carboxylate ligands or the hydroxamate inhibitor. The number of additional second coordination sphere C atoms added provides an estimate of the number of carboxylate ligands in the active site in samples that do not involve the hydroxamate inhibitor.

The FEFF parameters calculated for the carboxylate and Im models were checked by using them to fit experimental EXAFS data obtained from the model complexes used in calculations. Using the fitting procedures described above, refined distances to atoms in the first coordination sphere were within ± 0.02 Å of the crystallographic distances, and distances for second and third coordination sphere atoms were within ± 0.04 Å (e.g., see Table 4).

RESULTS AND DISCUSSION

Redox Chemistry. Although the biological function of GlxI does not involve a redox reaction, changes in the ligand environment, such as the addition of inhibitors that bind to the Ni, will influence the electron density at the Ni center and can potentially alter the oxidation state of the metal. These effects can be addressed by examining the Ni K-edge energy. Nickel K-edge XAS spectra result from the ejection of a 1s core electron into the continuum, which occurs at 8331.6 eV for Ni metal and near 8340 eV in Ni(II) model compounds (*34*). Since the energy required to dissociate a 1s core electron is influenced by the valence electron configuration, the edge energy provides a measure of the relative electron density on the Ni atom in different samples. As a result, changes in electron density between structurally similar compounds can provide information regarding oxidation state changes. A one electron oxidation state change typically results in at least a 2 eV shift in the edge energy, assuming a constant ligand environment (*25*, *35*, *36*).

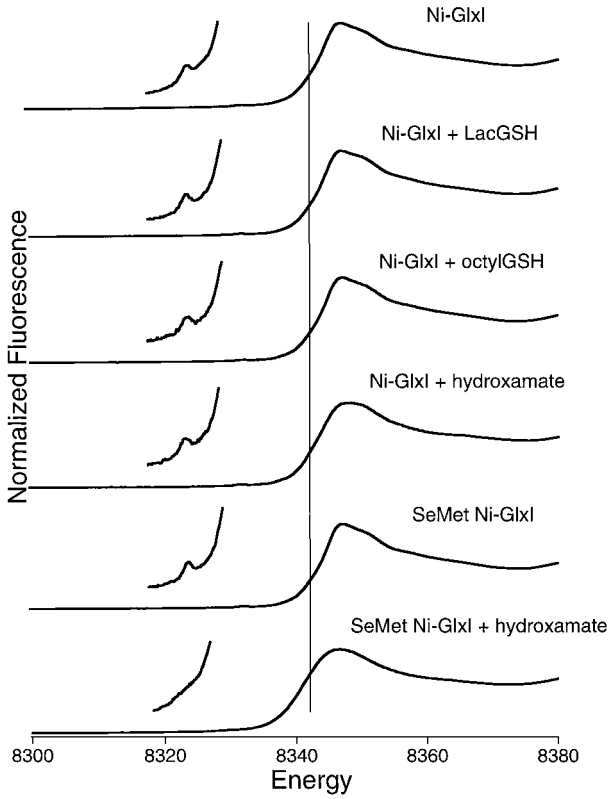

FIGURE 2: Ni K-edge XAS of *E. coli* Ni-GlxI and SeMet Ni-GlxI samples. Inserts are expansions of the preedge XANES region showing the 1s → 3d transitions.

The Ni K-edge XAS spectra, showing the edge region and X-ray absorption near-edge structure (XANES) features associated with *E. coli* GlxI, are summarized in Table 1 and Figure 2. With the exception of the SeMet Ni-GlxI hydroxamate complex, all samples have the same edge energy within experimental error. This result is consistent with the nonredox function of this enzyme. Since none of the samples exhibit electron paramagnetic resonance (EPR) signals associated with an $S = 1/2$ Ni species, it is likely that Ni is always in the +2 oxidation state, and no redox process is expected to take place upon addition of inhibitors or upon substitution of SeMet for Met. The SeMet Ni-GlxI hydroxamate complex has an edge energy 1.7 eV below that of the SeMet Ni-GlxI sample. A change of this magnitude could be ascribed to a one-electron oxidation state change; however, the SeMet Ni-GlxI hydroxamate complex does not exhibit an EPR signal that would be expected for reduction to Ni(I). The possible binding of Se (a

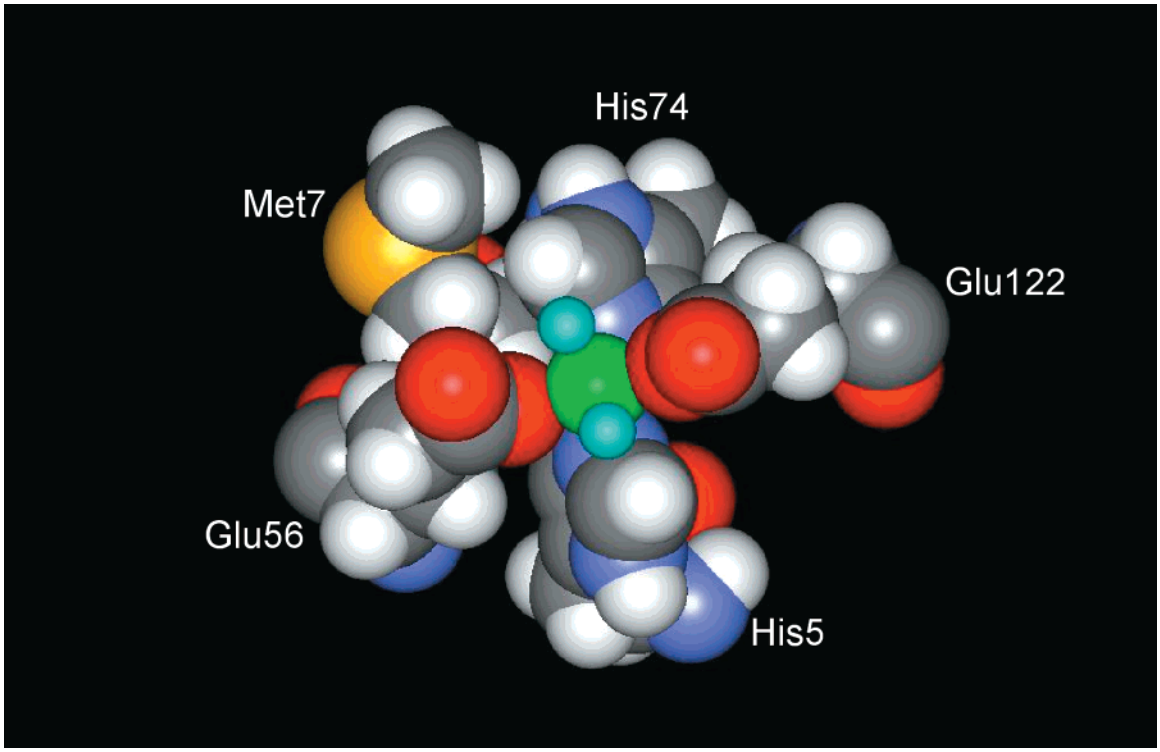

FIGURE 3: *E. coli* Ni-GlxI active site showing Ni^{2+} (green), two oxygen atoms of the aqua ligands (cyan, shown in half its diameter for clarity), the four metal binding ligands (His5, Glu56, His 74, and Glu122), and the proximal Met7. Graphics generated using WebLab ViewerPro, ver 3.7 (Molecular Simulations Inc.)

soft donor atom) to Ni is ruled out by EXAFS analysis (vide infra). The substitution of one or more anionic ligands (e.g., hydroxamate) for a neutral ligand (e.g., H_2O) is a plausible explanation for the shift in Ni K-edge energy to lower values.

Coordination Number and Geometry. Information regarding the coordination number and geometry of the Ni sites in Ni-GlxI can be found in the XANES region of the spectrum. In addition to the wild-type nickel enzyme, the selenomethionine derivative of *E. coli* GlxI where Met1, 7, and 26 were replaced with SeMet was studied. This derivative has a slightly modified V_{max} (435 ± 9 μmol min^{-1} mg^{-1} versus 676 ± 17 μmol min^{-1} mg^{-1} for wild-type GlxI) but unchanged K_m (23 ± 2.3 μM versus 27.2 ± 0.4 μM for wild-type). Since SeMet does not often alter enzyme kinetics, the structural perturbation due to incorporation of SeMet was of interest, particularly in view of the *E. coli* GlxI crystal structure, which indicates that Met7 is proximal to the metal ligands His 5 and Glu56 (Figure 3). The XANES region is sensitive to the number of ligands and the geometry of the ligands bound to the metal site. Although EXAFS analysis can be used to determine the number of donor atoms, its accuracy is limited to $\pm$ 25% due to correlations between the number of donor ligands and the disorder (σ^2) in the M-L distances. Thus, XANES analysis provides a more reliable determination of the geometry and number of ligands. XANES features in the XAS spectrum occur as a result of high energy electronic transitions from the 1s core to unoccupied metal valence orbitals. The 1s $\rightarrow$ 3d transition, which is observed near 8332 eV in Ni(II) model complexes, is a weak feature in the XANES region and provides an indication of the geometry of the metal site. This transition is formally forbidden in centrosymmetric environments, but gains intensity from p−d orbital mixing in noncentrosymmetric complexes. Such mixing of orbital character is maximal for tetrahedral geometry (1s $\rightarrow$ 3d peak areas $\sim 10 \times 10^{-2}$ eV), and minimal for six-coordinate and four-coordinate planar geometries (peak areas $= 0-4 \times 10^{-2}$ eV), with five-coordinate complexes having intermediate peak areas ($5-7 \times 10^{-2}$ eV) (*25*, *37*). The six- and four-coordinate planar environments can be distinguished by the presence (planar) or absence (octahedral) of a resolved peak at $\sim$8338 eV, which is associated with a 1s $\rightarrow$ $4p_z$ transition (with shakedown contributions) (*25*, *37*). This transition is also observed in five-coordinate square pyramidal (*25*) and distorted square planar complexes (*38*), but not in five-coordinate trigonal bipyramidal complexes (*25*).

Since none of the Ni-GlxI samples exhibits either a resolved 1s $\rightarrow$ $4p_z$ peak, or a shoulder on the edge, it can be concluded that neither a square planar nor a five-coordinate square pyramidal geometry is present in the Ni-GlxI samples. The magnitude of the 1s $\rightarrow$ 3d transitions in all samples, with the exception of the Ni-GlxI hydroxamate complex, are small and range from $(1.5-3.8) \times 10^{-2}$ eV. Since no 1s $\rightarrow$ $4p_z$ transitions are observed, it can be concluded that the Ni sites in these samples are all six-coordinate. However, the Ni-GlxI hydroxamate complex exhibits a 1s $\rightarrow$ 3d transition peak whose magnitude is more consistent with a five-coordinate geometry ($5.1(4) \times 10^{-2}$ eV). Since the edge structure is devoid of a 1s $\rightarrow$ $4p_z$ feature, a trigonal bipyramidal geometry is indicated. This suggests that a ligand associated with the Ni site in the native sample is lost upon addition of hydroxamate.

The results from Ni K-edge and XANES analysis combined suggest that addition of LacGSH or OctylGSH to Ni-GlxI has no effect on either the redox level or the geometry

of the Ni site. This confirms that the OctylGSH does not directly interact with the metal, as expected. Crystallization of the *H. sapiens* GlxI enzyme in the presence of hexylglutathione also did not appear to significantly alter the metal ligand environment (*15*). In contrast, EPR and NMR studies on the *H. sapiens* GlxI enzyme suggested that the addition of LacGSH removes one water ligand from the metal environment (*19*). There is no evidence for this in *E. coli* Ni-GlxI, under the given conditions.

This conclusion can also be made when comparing Ni-GlxI with SeMet Ni-GlxI. In contrast, the addition of hydroxamate to either Ni-GlxI or SeMet Ni-GlxI changes the Ni site but in distinct ways. In Ni-GlxI, a ligand appears to be lost upon addition of hydroxamate, but little change in the Ni K-edge energy is observed. In SeMet Ni-GlxI, addition of hydroxamate results in an increase in electron density (decrease in edge energy) at the Ni site without a change in the number of ligands. The substitution of a more electron-rich ligand for a less electron-rich ligand may account for this observation, such as the substitution of hydroxamate for two H_2O molecules.

The Ligand Environment. The ligand environment can be probed by analysis of the EXAFS region of the spectrum, which provides information about the types of donor atoms involved and metric details of the metal site structure (*39*). EXAFS results from the oscillation in the X-ray absorption coefficient produced by scattering of the ejected photoelectron. The results from iterative fitting of EXAFS using Fourier-filtered data with a backtransform window of 1.1−4.0 Å are summarized in Tables 2 and 3, and in Figures 4 and 5. Table 2 shows the best single shell fit, which indicates the presence of only O or N-donor ligands (modeled as O atoms). Selected two shell fits, fits incorporating a set of histidine ligands (two refined distances), and the best fits incorporating histidine ligands and Ni-C vectors from carboxylate C atoms (e.g., for Asp, Glu, three refined distances) are also shown.

It can be seen from Table 2 that the best single shell fits contain 5/6 O/N donor ligands at an average distance of 2.06(4) Å (fits A01, B01, C01, D01, D02, E01, and F01). Minor improvements in the fits are observed by splitting the O/N donors into two shells in all cases except for the SeMet Ni-GlxI hydroxamate complex. The fits of the Ni site in the Ni-GlxI, Ni-GlxI LacGSH complex, and Ni-GlxI OctylGSH complex are improved by modeling the site as six-coordinate with two shells of O/N donors composed of 1-2 O/N at 1.95(2) Å plus 4-5 O/N at 2.09(2) Å (fits A02, A03, B02, B03, C02, and C03). A comparison of the EXAFS results for the Ni-GlxI samples would suggest that the addition of LacGSH and OctylGSH has no effect on the first coordination sphere of Ni. Similar results are obtained when Ni-GlxI is compared with SeMet Ni-GlxI (fits A02 vs E02 and A03 vs E03). The possibility that Se binds to Ni was addressed by adding a shell of Se atoms to the two shell O atom fits. Although this leads to an improvement in the fit (fit E05), the refined Ni-Se distance is considerably longer than normal primary coordination sphere Ni-Se distances observed in model compounds (fit E05; 2.8 vs 2.4 Å in model systems) (*40*−*42*). Since the first coordination sphere of the Ni site is unchanged by the substitution of SeMet for Met in Ni-GlxI, it is likely that the active site is simply "crowded" by the larger Se atom, which may result in alteration of the catalytic rate of the enzymes. On the basis of the present EXAFS data, the introductions of the Se atom does not directly perturb the metal center. However, more distal effects on the active site outside the primary coordination sphere of the metal cannot be ruled out.

The Ni-GlxI hydroxamate complexes appear to exhibit different properties when compared with the other samples, as was observed in the XANES/K-edge analyses. Both the Ni-GlxI hydroxamate complex and the SeMet Ni-GlxI hydroxamate complex have slightly shorter average Ni-O/N distances than the other samples (fits D01, D02, and F01). The shorter average Ni-O/N distances coupled with the XANES analysis demonstrate that the primary coordination sphere of the Ni is altered by the presence of the hydroxamate inhibitor, likely indicating that it is a Ni ligand. The Ni-GlxI hydroxamate complex can be modeled using two shells of O/N donors [2 O/N at 1.92(3) Å and 3 O/N at 2.06(2) Å; fits D03, D04, D05]. When attempts were made to model the Ni site in SeMet Ni-GlxI hydroxamate complex with two shells of O/N donors, unacceptably large values of σ^2 were obtained (see Supporting Information, Table S8).

Multiple Scattering. The Fourier transformed EXAFS data reveals several peaks due to atoms outside the primary coordination sphere of the Ni (Figure 4). On the basis of the crystal structure of GlxI, these features can be attributed to histidine imidazole ligands with minor contributions from carboxylate C atoms. To fit EXAFS arising from histidine residues and carboxylate C atoms outside the primary coordination sphere of Ni, a method for fitting multiple scattering pathways for these atoms was devised. Using the *ab initio* program FEFF 6 (*28*−*30*), theoretical phase and amplitude parameters for both single and multiple scattering pathways involving second and third coordination sphere imidazole C and N atoms were obtained from a single Im ring from the crystallographically characterized model compound $[Ni(Im)_6](BF_4)_2$ (*32*). To limit the number of pathways and adjustable parameters involved in fits to a minimum, we employed only pathways that contributed more than 17% of the calculated intensity, constrained the number of distances adjusted to a single Ni-N distance, and limited the number of σ^2 values to four. (See Experimental Procedures). These parameters were then tested by using them to fit experimentally obtained XAS data from $[Ni(Im)_6](BF_4)_2$ by varying only the Ni-N distance and σ^2 values. The EXAFS fits obtained from $[Ni(Im)_6](BF_4)_2$ using the FEFF 6 parameters are shown in Figure 6 and Table 4, which also provides a comparison between the distances obtained from EXAFS analysis and crystallographic distances. The distances to atoms in the first, second, and third coordination sphere of Ni are in good agreement with crystallographic results despite the fact that the model uses a single Im ring tied to a single Ni-N distance to model the EXAFS of three crystallographically distinct Im rings in the model compound. The intensity of the EXAFS obtained from the model was more consistent with five Im ligands than six, but this is within the usual error for the number of similar ligands obtained from the analysis of the intensity of EXAFS arising from atoms in the primary coordination sphere (± 25%). This method of analysis is expected to approximate the number of Im ligands assuming that the Im ligands have similar M-N distances and that the rings are not distorted so as to significantly alter the multiple scattering pathways. In the case of *E. coli* GlxI,

Table 2: Selected Curve-Fitting Results of Filtered EXAFS Spectra for *Escherichia coli* Glyoxalase I[a,b]

sample	fit	*N* Ni−X[c]		*R* (Å)	σ^2 ($\times 10^3$ Å)[d]	$\Delta\sigma^2$ ($\times 10^3$ Å)	res (%)
Ni-GlxI	A01	6 Ni−O		2.0696(2)	7.0	2.4	35.6
	A02	1 Ni−O		1.9145(5)	0.2	−4.4	29.2
		5 Ni−O		2.0827(2)	2.9	−1.7	
	A03	2 Ni−O		1.9582(4)	3.3	−1.3	29.3
		4 Ni−O		2.1005(3)	1.8	−2.8	
	A04	4 Ni−O		2.0955(2)	1.4	−3.2	10.6
		2[His]	[Ni−N]	[1.9713(4)]	2.1	−2.5	
			[Ni−2C]	[2.9295(4)]	0.7	−4.8	
				[3.0127(4)]			
			[Ni−C/N]	[4.1025(4)]	25.8	20.3	
				[4.1557(4)]			
	A05	4 Ni−O		2.1004(3)	1.6	−3.0	8.9
		2[His]	[Ni−N]	[1.9841(4)]	2.0	−2.6	
			[Ni−2C]	[2.9423(4)]	4.0	−1.5	
				[3.0255(4)]			
			[Ni−C/N]	[4.1153(4)]	*10.5*	5.0	
				[4.1685(4)]			
		2{Glu}	{Ni−C}	{2.940(2)}	1.6	−3.9	
Ni-GlxI LacGSH complex	B01	6 Ni−O		2.0601(2)	8.9	4.3	33.6
	B02	1 Ni−O		1.9161(5)	1.2	−3.4	29.5
		5 Ni−O		2.0792(2)	4.7	0.1	
	B03	2 Ni−O		1.9557(4)	3.8	−0.8	29.6
		4 Ni−O		2.0990(3)	3.4	−1.2	
	B04	4 Ni−O		2.0959(3)	2.8	−1.8	10.4
		2[His]	[Ni−N]	[1.9725(3)]	2.3	−2.3	
			[Ni−2C]	[2.9307(3)]	3.1	−2.4	
				[3.0139(3)]			
			[Ni−C/N]	[4.1307(3)]	*17.2*	11.7	
				[4.1569(3)]			
	B05	4 Ni−O		2.0979(3)	3.2	−1.4	8.8
		2[His]	[Ni−N]	[1.9815(4)]	2.6	−2.0	
			[Ni−2C]	[2.9397(4)]	4.1	−1.4	
				[3.0229(4)]			
			[Ni−C/N]	[4.1127(4)]	*14.6*	9.1	
				[4.1659(4)]			
		2{Glu}	{Ni−C}	{2.897(4)}	3.1	−2.4	
Ni-GlxI OctylGSH complex	C01	6 Ni−O		2.0606(1)	*10.1*	5.5	30.8
	C02	1 Ni−O		1.9262(4)	5.2	0.6	29.1
		5 Ni−O		2.0782(1)	6.8	2.2	
	C03	2 Ni−O		1.9710(4)	8.0	3.4	29.2
		4 Ni−O		2.0925(3)	6.1	1.5	
	C04	4 Ni−O		2.0950(2)	4.4	−0.2	7.0
		2[His]	[Ni−N]	[1.9773(2)]	4.3	−0.3	
			[Ni−2C]	[2.9355(2)]	4.0	−1.5	
				[3.0187(2)]			
			[Ni−C/N]	[4.1085(2)]	*23.5*	18.0	
				[4.1617(2)]			
	C05	4 Ni−O		2.0959(2)	4.7	0.1	6.0
		2[His]	[Ni−N]	[1.9838(3)]	4.7	0.1	
			[Ni−2C]	[2.9420(3)]	6.1	0.6	
				[3.0252(3)]			
			[Ni−C/N]	[4.1150(3)]	*20.8*	15.3	
				[4.1682(3)]			
		2{Glu}	{Ni−C}	{2.932(4)}	6.5	1.0	
Ni-GlxI Hox complex	D01	5 Ni−O		2.0212(1)	6.8	2.2	28.4
	D02	6 Ni−O		2.0218(1)	8.8	4.2	29.2
	D03	2 Ni−O		1.9400(2)	0.8	−3.8	25.8
		3 Ni−O		2.0769(2)	1.0	−3.6	
	D04	1 Ni−O		1.8980(6)	5.3	0.7	27.3
		5 Ni−O		2.0384(2)	6.1	1.5	
	D05	2 Ni−O		1.9374(5)	6.8	2.2	27.2
		4 Ni−O		2.0535(4)	5.2	0.6	
	D06	5 Ni−O		2.0313(4)	7.0	2.4	15.4
		1[His]	[Ni−N]	[1.9480(8)]	*10.1*	5.5	
			[Ni−2C]	[2.9062(8)]	6.5	1.0	
				[2.9894(8)]			
			[Ni−C/N]	[4.0792(8)]	7.4	1.9	
				[4.1324(8)]			
	D07	4 Ni−O		2.0625(2)	3.2	−1.4	11.8
		2[His]	[Ni−N]	[1.9484(3)]	2.0	−2.6	
			[Ni−2C]	[2.9066(3)]	8.6	3.1	
				[2.9898(3)]			

Table 2 (Continued)

sample	fit	*N* Ni−X[c]		*R* (Å)	σ^2 (× 10^3 Å)[d]	$\Delta\sigma^2$ (× 10^3 Å)	res (%)
			[Ni−C/N]	[4.0796(3)]	*20.3*	14.8	
				[4.1328(3)]			
	D08	4 Ni−O		2.0586(3)	4.0	−0.6	10.2
		2[His]	[Ni−N]	[1.9542(4)]	3.4	−1.2	
			[Ni−2C]	[2.9124(4)]	*16.4*	10.9	
				[2.9956(4)]			
			[Ni−C/N]	[4.0854(4)]	*18.6*	13.1	
				[4.1386(4)]			
		{Hox}	{Ni−2C}	{2.832(2)}	1.5	−4.0	
				{2.966(2)}			
SeMet Ni-GlxI	E01	6 Ni−O		2.0628(1)	7.8	3.2	33.3
	E02	1 Ni−O		1.9391(2)	1.1	−3.5	31.5
		5 Ni−O		2.0844(1)	4.5	−0.1	
	E03	2 Ni−O		1.9740(2)	3.1	−1.5	31.6
		4 Ni−O		2.1033(1)	3.4	−1.2	
	E04	4 Ni−O		2.1000(1)	2.6	−2.0	10.0
		2[His]	[Ni−N]	[1.9879(1)]	1.5	−3.1	
			[Ni−2C]	[2.9461(1)]	0.5	−5.0	
				[3.0293(1)]			
			[Ni−C/N]	[4.1191(1)]	*16.1*	10.6	
				[4.1723(1)]			
	E05	2 Ni−O		1.9836(3)	4.7	0.1	20.7
		4 Ni−O		2.0988(2)	4.5	−0.1	
		1 Ni−Se		2.8861(2)	7.2	5.7	
	E06	4 Ni−O		2.1033(2)	3.0	−1.6	7.8
		2[His]	[Ni−N]	[1.9979(3)]	1.6	−3.0	
			[Ni−2C]	[2.9561(3)]	2.1	−3.4	
				[3.0393(3)]			
			[Ni−C/N]	[4.1291(3)]	*13.5*	8.0	
				[4.1823(3)]			
		2{Glu}	{Ni−C}	{2.931(3)}	2.1	−3.4	
	E07	4 Ni−O		2.1047(2)	2.5	−2.1	6.3
		1 Ni−Se		2.880(1)	6.3	4.8	
		2[His]	[Ni−N]	[1.9907(3)]	9.0	4.4	
			[Ni−2C]	[2.9489(3)]	*17.9*	12.4	
				[3.0321(3)]			
			[Ni−C/N]	[4.1219(3)]	*14.0*	8.5	
				[4.1751(3)]			
		2{Glu}	{Ni−C}	{2.708(3)}	*10.7*	5.2	
SeMet GlxI Hox complex	F01	6 Ni−O		2.0296(1)	*11.6*	7.0	24.0
	F02	1 Ni−O		2.0245(3)	2.3	−2.3	22.5
		5 Ni−O		2.0334(3)	*15.4*	10.8	
	F03	2 Ni−O		2.0240(2)	4.9	0.3	22.5
		4 Ni−O		2.0398(5)	*18.0*	13.4	
	F04	5 Ni−O		2.0475(3)	9.9	5.3	8.6
		1[His]	[Ni−N]	[1.9677(8)]	6.8	2.2	
			[Ni−2C]	[2.9259(8)]	7.7	2.2	
				[3.0091(8)]			
			[Ni−C/N]	[4.0989(8)]	*11.1*	5.6	
				[4.1521(8)]			
	F05	4 Ni−O		2.0688(3)	7.3	2.7	8.0
		2[His]	[Ni−N]	[1.9704(5)]	5.8	1.2	
			[Ni−2C]	[2.9286(5)]	*11.8*	6.3	
				[3.0118(5)]			
			[Ni−C/N]	[4.1016(5)]	*30.1*	24.6	
				[4.1548(5)]			
	F06	5 Ni−O		2.0452(3)	*10.7*	6.1	6.9
		1[His]	[Ni−N]	[1.9908(8)]	6.8	2.2	
			[Ni−2C]	[2.9490(8)]	3.1	−2.4	
				[3.0322(8)]			
			[Ni−C/N]	[4.1220(8)]	7.0	1.5	
				[4.1752(8)]			
		1{Glu}	{Ni−C}	{2.849(1)}	0.6	−4.9	
	F07	5 Ni−O		2.0542(3)	*10.7*	6.1	7.3
		1[His]	[Ni−N]	[1.991(1)]	7.1	2.5	
			[Ni−2C]	[2.949(1)]	*10.9*	5.4	
				[3.033(1)]			
			[Ni−C/N]	[4.122(1)]	7.0	1.5	
				[4.176(1)]			
		2{Glu}	{Ni−C}	{2.901(5)}	9.0	3.5	
	F08	4 Ni−O		2.0670(4)	7.6	3.0	6.3
		2[His]	[Ni−N]	[1.9748(7)]	6.4	1.8	

Table 2 (Continued)

sample	fit	*N* Ni−X[c]		*R* (Å)	σ^2 (× 10^3 Å)[d]	$\Delta\sigma^2$ (× 10^3 Å)	res (%)
			[Ni−2C]	[2.9330(7)]	*16.4*	10.9	
				[3.0162(7)]			
			[Ni−C/N]	[4.1060(7)]	*26.6*	21.1	
				[4.1592(7)]			
		2{Glu}	{Ni−C}	{2.915(4)}	9.9	4.4	
	F09	5 Ni−O		2.0442(3)	*11.0*	5.5	4.7
		1[His]	[Ni−N]	[1.999(1)]	7.3	2.7	
			[Ni−2C]	[2.957(1)]	*15.3*	9.8	
				[3.040(1)]			
			[Ni−C/N]	[4.130(1)]	6.2	0.7	
				[4.183(1)]			
		{Hox}	{Ni−2C}	{2.822(2)}	4.7	−0.8	
				{2.956(2)}			
	F10	4 Ni−O		2.0650(5)	8.0	3.4	6.2
		2[His]	[Ni−N]	[1.9781(8)]	7.0	2.4	
			[Ni−2C]	[2.9363(8)]	*18.2*	12.7	
				[3.0195(8)]			
			[Ni−C/N]	[4.1093(8)]	*26.2*	20.7	
				[4.1625(8)]			
		{Hox}	{Ni−2C}	{2.824(2)}	7.5	2.0	
				{2.959(2)}			

[a] Data range, $k = 2-12.5$ Å^{-1}, BT window = 1.1−4.0 Å. [b] X is the scattering atom for each shell; *R* is the Ni-X distance; σ^2 is the root-mean-square disorder in the Ni−X distance; $\Delta\sigma^2$ is σ^2 relative to calculated values for reference compounds; res (%) is the residual as defined in the Experimental Procedures. The accuracy of distances determined by EXAFS for atoms in the first coordination sphere of the metal are limited to ± 0.02 Å by the theoretical phase parameters. The refinements generally show precisions that are less than 0.02 Å for well-ordered shells, and thus differences in distances between samples using equivalent fits are more accurate than the absolute distances. [c] The distances shown are for the single scattering pathways used in the fits of Ni-GlxI. Histidine (His) ligands were fit using single and multiple scattering pathways for $Ni(Im)_6(BF_4)_2$ obtained from FEFF 6. The distances obtained from these pathways were then correlated such that the imidazoles fit as a single unit and the data refined. The Ni-His distances obtained for the GlxI fits are enclosed in brackets to denote that these distances were correlated. Similarly, the distances for the single and multiple scattering pathways obtained from $[Ni(sal)_2(H_2O)_2]$ and $[Ni(lac)_2(tmen)]$ were also correlated to fit second coordination sphere C atoms to the Ni-GlxI data. Distances obtained are shown in braces to denote that the pathways used were refined as a unit. [d] Italicized values are approaching physical insignificance. Large values of σ^2 suggest that the shell involved has a coordination number that is too large or is badly disordered and may be unnecessary for fitting the data.

Table 3: Summary of EXAFS Fitting Results for *Escherichia coli* GlxI

sample[a]	ave Ni−O/N (Å)[b]	no. of His ligands
Ni-GlxI	2.07(2)	2
Ni-GlxI LacGSH complex	2.06(2)	2
Ni-GlxI OctylGSH complex	2.06(2)	2
Ni-GlxI Hox complex	2.02(2)	2
SeMet Ni-GlxI	2.06(2)	2
SeMet Ni-GlxI Hox complex	2.03(2)	1−2

[a] Hox refers to the transition state analogue inhibitor L-(-glutamyl-*N*-hydroxy-*N*-methyl-L-glutaminylglycine. [b] The average Ni-O/N distances were taken from the single shell fits.

the enzyme contains only two His residues (*11*). Thus, the only possibilities are 0, 1, or 2 His ligands, with a minimum difference of 50%.

Replacement of a shell of O/N donors in the two shell fits by His imidazole ligands greatly improves the fits for all the Ni-GlxI samples. Incorporation of one His imidazole in the fits led to negative values of σ^2 for some of the atoms in the imidazole ring in all samples except the hydroxamate complexes (see Table 2 and Supporting Information). Negative values of σ^2 are physically meaningless and indicate that the number of scattering atoms in that shell is too small. The "best" fits were found with the addition of two His ligands (fits A04, B04, C04, and D07) with very similar distances (1.97 ± 0.02 Å) obtained in the different samples, a result that is consistent with the crystal structure of the native enzyme (*17*). Thus, no effect on the His ligands is observed upon addition of either product or inhibitors. SeMet Ni-GlxI also fits better with two His residues (fit E04). The distances obtained for the His ligands are essentially the same as those for Ni-GlxI, and thus substitution of SeMet for Met does not appear to affect the coordination of the His residues at the Ni active site and, therefore, is not the source of the lowered enzyme activity in SeMet Ni-GlxI. For the SeMet Ni-GlxI hydroxamate complex, EXAFS does not distinguish well between one and two histidine ligands (compare fits F04, F05; F09; F10). However, the XANES analysis indicates that the Ni site is still six-coordinate and EXAFS analysis indicates only N/O donor ligands are present. Given the fact that the average Ni-N(His) distance (1.97(2) Å) is identical to those obtained from the analysis of the other samples, the data favor retention of both His ligands in the SeMet Ni-GlxI hydroxamate complex.

Previous studies on Ni-GlxI indicated that EXAFS fits could be further improved by the addition of a shell of Ni-C atoms from the C_α of carboxylate amino acid residues (e.g., Glu) in the active site (fit A05) (*16*). The improvements in the fits upon addition of a shell of C atoms in the second coordination sphere of the Ni is minor and at the level of the noise in the data (see Supporting Information). The Ni-GlxI samples with LacGSH or OctylGSH added are best fit by the addition of two C atoms (fits B05 and C05). Addition of a shell of Ni-C atoms to SeMet Ni-GlxI containing a shell of His ligands also leads to minor improvement in the fits (Fit E06). The Ni-C_{carbox} distances in these samples are the same as those observed in Ni-GlxI (2.92 ± 0.02 Å). This result is consistent with the conclusion that the overall structure of Ni-GlxI is essentially unchanged by the addition of either LacGSH or OctylGSH, or by SeMet substitution.

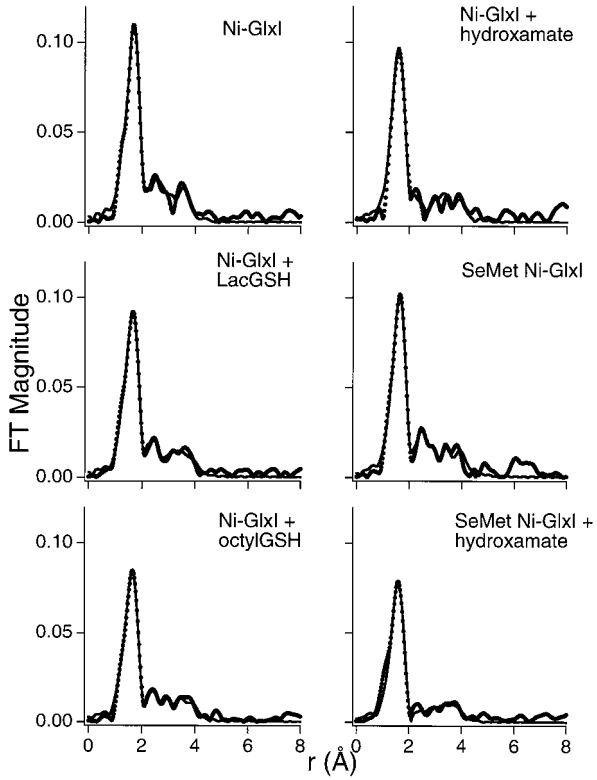

FIGURE 4: Fourier transformed (k = 2.0−12.5 Å^{-1}) Ni K-edge EXAFS spectra from *E. coli* Ni-GlxI and SeMet Ni-GlxI samples (circles) and fits (solid line). The fits shown correspond to fits A05, B05, C05, D08, E06, and F07 in Table 2.

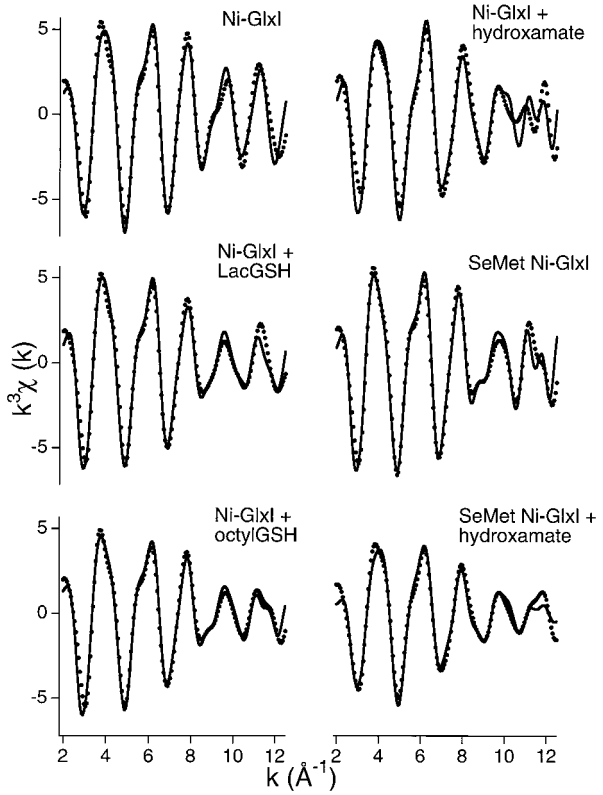

FIGURE 5: Fourier-filtered (back transform window, r = 1.1−4.0 Å, uncorrected for phase shifts), Ni K-edge EXAFS spectra from *E. coli* Ni-GlxI and SeMet Ni-GlxI samples (circles) and fits (solid line). The fits shown correspond to fits A05, B05, C05, D08, E06, and F07 in Table 2.

Mechanistic Insights. Three plausible mechanisms of Ni-GlxI catalysis are outlined in Schemes 2−4. Scheme 4, which features an unidentified amino acid side chain as a catalytic base, can be discounted on the basis of the Ni-GlxI crystal structure, which shows no residue that could be a candidate for a catalytic base in reasonable proximity to the Ni site. Mechanisms 2 and 3 can be distinguished in two ways. In mechanism 2, the substrate binds to the Ni center and displaces both waters and a Glu residue, which then serves as a catalytic base. In mechanism 3, the substrate does not bind to the Ni center and does not displace any ligands. Instead, the metal serves to ionize one aqua ligand to a hydroxo ligand, which then serves as the catalytic base.

The crystal structure of human GlxI with a different transition state analogue inhibitor (*S*-(*N*-hydroxy-*N*-*p*-iodophenylcarbamoyl)glutathione) added indicates that two water molecules and Glu172 are replaced by two O atoms from the inhibitor (*14*). The EXAFS data for Ni-GlxI are consistent with this result, although it is not clear whether hydroxamate displaces a carboxylate ligand in addition to the two water molecules. The XANES analysis showing a five-coordinate site is consistent with a [Ni(His)$_2$(Glu)(Hox)] five-coordinate structure. Such a structure is also consistent with the reaction mechanism that features displacement of a Glu ligand, which can then function as a catalytic base (Scheme 2) (*14*). However, the hydroxamate (pK_a 8−10) probably binds as an anion to the Ni complex, and maintenance of charge neutrality would be expected to result in the loss of an anionic ligand, such as Glu 122. The substrate (the expected pK_a of the hydroxyl group may well be >15 for an alkoxide) cannot exist as an anion near physiological pH and is thus unlikely to displace an anionic ligand. In fact, as a much weaker chelator, it may not bind to the metal at all, and thus the structure of the hydroxamate complex may be a poor model of enzyme−substrate interaction. Similarly,

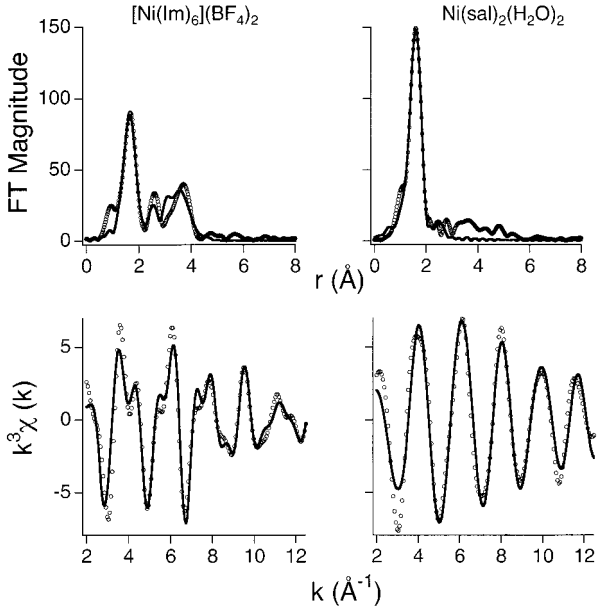

FIGURE 6: Fourier transformed (upper, k = 2.0−12.5 Å^{-1}) and Fourier-filtered (lower, back transform window, r = 1.1−4.0 Å, uncorrected for phase shifts) Ni K-edge EXAFS data for [Ni(Im)$_6$](BF$_4$)$_2$ (left) and [Ni(sal)$_2$(OH$_2$)$_2$] (right). Data are shown as circles, and best fits are shown as solid lines. The fits shown are from Table 4.

Table 4: Curve-Fitting Results of Filtered EXAFS Spectra for $Ni(Im)_6(BF_4)_2$ and $Ni(sal)_2(OH_2)_2$

compound	N	Ni−X	*R* (Å) {average}	σ^2 (× 10^3 Å)	$\Delta\sigma^2$ (× 10^3 Å)	res (%)	ave crystallogr distance (Å)
$Ni(Im)_6(BF_4)_2$	5	Ni−N	2.1064(1)	5.1	0.5	43.8	
	5	Im[Ni−N]	2.1097(1)	5.0	0.4	14.4	
	5	[Ni−2C]	3.0679(1)	5.3	−0.2		
			3.1511(1)				
	5	[Ni−C/N]	4.2409(1)	6.6	1.1		
			4.2941(1)				
	6	Ni−N	2.1075(1)	6.9	2.3	44.2	
	6	Im [Ni−N]	2.1107(1)	6.8	2.2	15.8	2.128
	6	[Ni−2C]	3.0689(1)	7.1	1.6		3.15
			3.1521(1)				
			{3.1105}				
	6	[Ni−C/N]	[4.2419(1)]	8.5	3.0		4.30
			[4.2951(1)]				
			{4.2685}				
$Ni(sal)_2(OH_2)_2$	6	Ni−O	2.0193(1)	4.6	0	16.7	
	6	Ni−O	2.0197(1)	4.6	0	15.9	2.028
	2	Ni−C	2.8559(1)	2.1	−3.4		2.90

Scheme 6

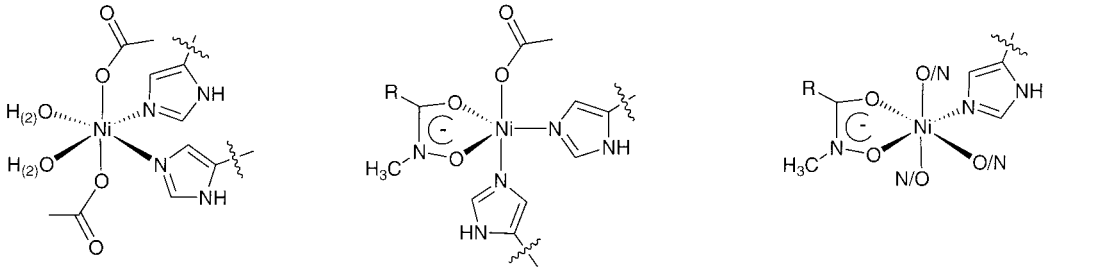

if the enediolate intermediate is short-lived, ligand exchange reactions may not occur. The lack of an enzyme−substrate interaction is also supported by the XAS results of the enzyme−product complex, which shows no perturbation of the active site Ni structure in the presence of the lactate thioester. Thus, the mechanism in Scheme 3, involving proton transfers between the substrate and a hydroxo and aqua ligands is favored. This mechanism is analogous to those proposed for proline and glutamate racemase (*43*, *44*), where a thiol/thiolate pair derived from Cys residues serves the function analogous to the hydroxo/aqua ligands in Ni-GlxI. The mechanism illustrated in Scheme 3 also requires that both aqua ligands be present on the metal, a feature that may explain why Zn-substituted Ni-GlxI with only one aqua ligand in the *E. coli* enzyme is catalytically inactive (*16*, *17*). Another implication from these studies is that the hydroxamate ligand is a poor transition state analogue because it binds to the Ni center displacing the catalytic water molecules and therefore does not resemble the transition state proposed in Scheme 3.

CONCLUSIONS

The results from XAS analyses of six different samples of *E. coli* Ni-GlxI lead to the following conclusions, which are summarized in Scheme 6.

(i) Ni K-edge energy analysis indicates that no redox processes take place upon addition of either product or inhibitor complexes, or when SeMet is substituted for Met. SeMet Ni-GlxI does show an increase in electron density at the Ni site when the hydroxamate is added, but this is not due to the reduction of Ni(II) to Ni(I). Instead, it is due to the substitution of the negatively charged hydroxamate for two water molecules, leading to an increase in the electron density (decrease in edge energy) on the Ni.

(ii) Addition of LacGSH or OctylGSH to Ni-GlxI does not have a major effect on the coordination environment of the Ni, indicating a nonbinding role for these compounds. However, addition of hydroxamate to Ni-GlxI results in the substitution of water molecules, as reflected by a decrease in ave Ni-O/N bond length and a decrease in coordination number from six to five, with the apparent loss of a carboxylate ligand.

(iii) Substitution of SeMet for Met results in an enzyme that has only ∼65% activity relative to Ni-GlxI. With the exception of a broader range of distances, little structural perturbation of the Ni site is detected by XAS. Thus, the loss of activity may result from a crowding of the substrate binding site induced by the presence of the larger Se atom.

(iv) A mechanism wherein the substrate does not bind to the metal center and where catalysis is achieved via the aqua ligands coordinated to the Ni site is consistent with the available structural data. This mechanism is analogous to those proposed for proline and glutamate racemases, where cysteine thiol/thiolate pairs serve a function analogous to hydroxo/aqua Ni ligands in Ni-GlxI.

ACKNOWLEDGMENT

We thank Mr. Hoa Ly for the preparation of the hydroxamate transition state analogue. The National Synchrotron Light Source (NSLS) at Brookhaven National Laboratory is supported by the U. S. Department of Energy, Division of Materials Sciences and Division of Chemical Sciences. Beamline X9B at NSLS is supported in part by NIH Grant RR-01633.

SUPPORTING INFORMATION AVAILABLE

Table S1 of FEFF 6 pathways obtained from $[Ni(Im)_6](BF_4)_2$. Table S2 of FEFF 6 pathways obtained from $[Ni(sal)_2(H_2O)_2]$ and $[Ni(lac)_2(tmen)]$. Tables S3−S8 of fits of Ni K-edge Fourier-filtered EXAFS data for the Glyoxalase I samples featured in this paper. Figure S1, Fourier transformed difference spectra for NiGlxI (52 pages). This material is available free of charge via the Internet at http://pubs.acs.org.

REFERENCES

1. Inoue, Y., and Kimura, A. (1995) *Advances in Microbial Physiology* (R. K. Poole, Ed.) pp 177−227, Vol. 37, Academic Press, London.
2. Cooper, R. A., and Anderson, A. (1970) *FEBS Lett. 11*, 273−276.
3. Ferguson, G. P., Tötemeyer, S., MacLean, M. J., and Booth, I. R. (1998) *Arch. Microbiol. 170*, 209−219.
4. Oya, T., Hattori, N., Mizuno, Y., Miyata, S., Maeda, S., Osawa, T., and Uchida, K. (1999) *J. Biol. Chem.* 18492−18502.
5. Thornalley, P. J. (1998) *Chem. Biol. Interact. 111−112*, 137−151.
6. Nagao, M., Fujita, Y., Wakanayashi, K., Nukaya, H., Kosuge, T., and Sugimara, T. (1986) *Environ. Health Perspect. 67*, 89−91.
7. Vander Jagt, D. L. (1989) in *Coenzymes and Cofactors VIII: Glutathione Part A* (Dolphin, D., Poulson, R., and Avramovic, O., Eds.) pp 597−641, John Wiley and Sons Inc., New York.
8. Aronsson, A.-C., Marmstål, E., and Mannervik, B. (1978) *Biochem. Biophys. Res. Commun. 81*, 1235−1240.
9. Ridderström, M., and Mannervik, B. (1996) *Biochem. J. 314*, 463−467.
10. Saint-Jean, A. P., Phillips, K. R., Creighton, D. J., and Stone, M. J. (1998) *Biochemistry 37*, 10345−10353.
11. Clugston, S. L., Barnard, J. F. J., Kinach, R., Miedema, D., Ruman, R., Daub, E., and Honek, J. F. (1998) *Biochemistry 37*, 8754−8763.
12. Clugston, S. L., and Honek, J. F. (2000) *J. Mol. Evol. 50*, 491−495.
13. Cameron, A. D., Olin, B., Ridderström, M., Mannervik, B., and Jones, T. A. (1997) *EMBO J. 16*, 3386−3395.
14. Cameron, A. D., Ridderström, M., Olin, B., Kavarana, M. J., Creighton, D. J., and Mannervik, B. (1999) *Biochemistry 38*, 13480−13490.
15. Ridderström, M., Cameron, A. D., Jones, T. A., and Mannervik, B. (1998) *J. Biol. Chem. 273*, 21623−21628.
16. Davidson, G., Clugston, S. L., Honek, J. F., and Maroney, M. J. (2000) *Inorg. Chem. 39*, 2962−2963.
17. He, M. M., Clugston, S. L., Honek, J. F., and Matthews, B. W. (2000) *Biochemistry 39*, 8719−8727.
18. Hall, S. S., Doweyko, A. M., and Jordan, F. (1976) *J. Am. Chem. Soc. 98*, 7460−7461.
19. Sellin, S., Eriksson, L. E. G., and Mannervik, B. (1982) *Biochemistry 21*, 4850−4857.
20. Sellin, S., Rosevear, P. R., Mannervik, B., and Mildvan, A. S. (1982) *J. Biol. Chem. 257*, 10023−10029.
21. Davis, R. W., Botstein, D., and Roth, J. R. (1980) *Advanced Bacterial Genetics*, Cold Spring Harbor Laboratory, Cold Spring Harbor, NY.
22. Ly, H. D., Clugston, S. L., Sampson, P. B., and Honek, J. F. (1998) *Bioorg. Med. Chem. Lett. 8*, 705−710.
23. Stokvis, E., Clugston, S. L., Honek, J. F., and Heck, A. J. R. (2000) *J. Prot. Chem. 19*, 389−397.
24. Bagyinka, C., Whitehead, J. P., and Maroney, M. J. (1993) *J. Am. Chem. Soc. 115*, 3576−3585.
25. Colpas, G. J., Maroney, M. J., Bagyinka, C., Kumar, M., Willis, W. S., Suib, S. L., Mascharak, P. K., and Baidya, N. (1991) *Inorg. Chem. 30*, 920−928.
26. Ressler, T. (1997) *J. Physique IV 7*, C2−269.
27. Davidson, G., Choudhury, S. B., Gu, Z., Bose, K., Roseboom, W., Albracht, S. P. J., and Maroney, M. J. (2000) *Biochemistry 39*, 7468−7479.
28. Mustre de Leon, J., Rehr, J. J., Zabinsky, S. I., and Albers, R. C. (1991) *Phys. Rev. B44*, 4146−4156.
29. Rehr, J. J., and Albers, R. C. (1990) *Phys. Rev. B41*, 8139−8149.
30. Rehr, J. J., Zabinsky, S. I., and Albers, R. C. (1992) *Phys. Rev. Lett. 69*, 3397−3400.
31. Stewart, J. M., Lingafelter, E. C., and Breazeale, J. D. (1961) *Acta Crystallog. 14*, 888−891.
32. van Ingen Schenau, A. D. (1975) *Acta Crystallog. B 31*, 2736−2738.
33. Ahlgren, M., and Turpeinen, U. (1977) *Finn. Chem. Lett.*, 129−130.
34. Maroney, M. J., Colpas, G. J., Bagyinka, C., Baidya, N., and Mascharak, P. K. (1991) *J. Am. Chem. Soc. 113*, 3962−3972.
35. Maroney, M. J., Pressler, M. A., Mirza, S. A., Whitehead, J. P., Gurbiel, R. J., and Hoffman, B. M. (1995) *Adv. Chem. Ser. 246*, 21−60.
36. Kirby, J. A., Goodin, D. B., Wydrzynski, T., Robertson, A. S., and Klein, M. P. (1981) *J. Am. Chem. Soc. 103*, 5537−5542.
37. Eidsness, M. K., Sullivan, R. J., and Scott, R. A. (1988) in *The Bioinorganic Chemistry of Nickel* (Lancaster, J. R., Jr., Ed.) pp 73−91, VCH, New York.
38. Xia, J., Dong, J., Wang, S., Scott, R. A., and Lindahl, P. A. (1995) *J. Am. Chem. Soc. 117*, 7065−7070.
39. Scott, R. A. (1985) *Methods Enzymol. 117*, 414−459.
40. Baidya, N., Noll, B. C., Olmstead, M. M., and Mascharak, P. K. (1992) *Inorg. Chem. 31*, 2999−3000.
41. Marganian, C. A., Baidya, N., Olmstead, M. M., and Mascharak, P. K. (1992) *Inorg. Chem. 31*, 2992−2994.
42. Goldman, C. M., Olmstead, M. M., and Mascharak, P. K. (1996) *Inorg. Chem. 35*, 2752−2757.
43. Albery, W. J., and Knowles, J. R. (1986) *Biochemistry 25*, 2572−2577.
44. Glavas, S., and Tanner, M. E. (1999) *Biochemistry 38*, 4106−4113.

BI0018537